Bio-Medical Materials and Engineering 24 (2014) 1299–1306
DOI 10.3233/BME-130932
IOS Press

Numerical Analysis of the Effect of T-tubule Location on Calcium Transient in Ventricular Myocytes

Uduak Z. George, Jun Wang, and Zeyun Yu *,
Department of Computer Science, University of Wisconsin-Milwaukee, Milwaukee, WI 53211, U.S.A

Abstract. Intracellular calcium (Ca^{2+}) signaling in cardiac myocytes is vital for proper functioning of the heart. Understanding the intracellular Ca^{2+} dynamics would give an insight into the functions of normal and diseased hearts. In the current study, spatiotemporal Ca^{2+} dynamics is investigated in ventricular myocytes by considering Ca^{2+} release and re-uptake via sarcolemma and transverse tubules (T-tubules), Ca^{2+} diffusion and buffering in the cytosol, and the blockade of Ca^{2+} activities associated with the sarcoplasmic reticulum. This study is carried out using a three dimensional (3D) geometric model of a branch of T-tubule extracted from the electron microscopy (EM) images of a partial ventricular myocyte. Mathematical modeling is done by using a system of partial differential equations involving Ca^{2+} , buffers, and membrane channels. Numerical simulation results suggest that a lack of T-tubule structure at the vicinity of the cell surface could increase the peak time of Ca^{2+} concentration in myocytes. The results also show that T-tubules and mobile buffers play an important role in the regulation of Ca^{2+} transient in ventricular myocytes.

Keywords: Cardiac myocytes, calcium dynamics, reaction-diffusion equations, numerical analysis, finite element method

1. Introduction

Intracellular Ca^{2+} in cardiac myocytes is regulated by multiple interacting cellular systems that function within an integrative framework [2]. The ventricular myocyte is enclosed by the sarcolemma. The sarcolemma is a specialized structure that forms invaginations known as the transverse tubules (T-tubules) into the myocyte and opens freely to the extracellular space [3,4]. On the sarcolemma and T-tubule, there reside some ion channels that are important in communicating signals within and between cells [5]. These ion channels play an important role in transient changes in membrane potential that regulates E-C coupling [4]. The L-type Ca^{2+} channels (LCCs) are activated during cardiac action potential (AP), leading to an influx of Ca^{2+} into the cytosol, which triggers the release of Ca^{2+} from sarcoplasmic reticulum (SR) [2]. The prevalence of free Ca^{2+} encourages the binding of Ca^{2+} to cytosolic binding proteins (or buffers) which is vital for the spatiotemporal regulation of intracellular Ca^{2+} signals [2,6] and also

The work described was supported in part by an NIH Award (Number R15HL103497) from the National Heart, Lung, and Blood Institute (NHLBI) and by a grant from the UWM Research Growth Initiative.
*Corresponding author. E-mail: yuz@uwm.edu.

for the contraction of the myocyte. Ca^{2+} influx also occurs through the Na^{+}-Ca^{2+} exchangers (NCXs) which increases the cytostolic Ca^{2+} level [2]. NCXs are bidirectional channels and are one of the primary systems for Ca^{2+} efflux from the myocyte [2,3,7]. The direction of NCX depends on the amount of Na^{+} and Ca^{2+} on either side of the membrane and also on the membrane potential [3,7]. In addition to Ca^{2+} channels and buffers, other proteins such as Ca^{2+} transporters and pumps remove Ca^{2+} from the cytosol and aid in the regulation of intracellular Ca^{2+} signals [6]. The removal of Ca^{2+} ions from the cytosol lowers the concentration of Ca^{2+} ions and thereby leads to a relaxation of the myocyte.

Defects in Ca^{2+} regulation are due to various factors including, reductions in SR Ca^{2+} content, changes in action potential shape and SR Ca^{2+} release dysfunctioning. Results from recent studies show that t-tubule structural remodeling is directly linked to SR Ca^{2+} release dysfunctioning [20]. Their study highlights the need to understand the regulation and signalling of Ca^{2+} within microdomains along with its pathophysiological and therapeutic implications. In Lu *et al* [8], Cheng *et al* [9] and Yao *et al* [10], Ca^{2+} interactions and concentrations were studied with SR activity inhibited in order to assess the effect of the distribution of sarcolemma and T-tubule ion channels on Ca^{2+} regulation in myocytes. Results from these studies show that Ca^{2+} transient in myocytes could be influenced by variations in the distribution of ion channels along the sarcolemma and T-tubule. If the distribution of ion channels along the sarcolemma and T-tubule influences Ca^{2+} transients in myocytes, then structural remodeling or rearrangement of the T-tubule could also influence Ca^{2+} transients in myocytes. This would inadvertently affect the distribution of ion channels along the T-tubule.

The aim of this study is to investigate the effect of the positioning of the T-tubule on Ca^{2+} dynamics. This is motivated by the need to understand the pathophysiological implications of T-tubule remodeling/relocation on myocytes. This study is carried out by utilizing a mathematical model describing the Ca^{2+} interactions via the sarcolemma and the T-tubule of myocytes [8,10]. Numerical experiments are carried out on three separate geometric models incorporated with realistic T-tubule structures extracted from 3D electron microscopy images at a high resolution. The three geometric models are approximately of equal dimensions and differ in the location of the T-tubule structure. Numerical results show variations in the predicted Ca^{2+} transient profiles among the geometric models, suggesting the importance of T-tubule location on Ca^{2+} dynamics in myocytes.

2. Methodology

Experimental observations have shown that T-tubules have complex geometries with detailed network of tubular structures, large local variations in diameter and transverse-axial anatomies and protrusions in many directions with a diameter that varies from 20 to 450 nm [9,11,12,13]. In order to accurately model the T-tubule, it is necessary to develop realistic geometric models from 3D imaging data [9]. This study utilizes a topologically complicated and accurate T-tubule structure extracted from 3D electron microscopy images of a venticular myocyte at a high resolution (see Figure 1a). The surface area of this T-tubule is $4.39\mu m^2$. The T-tubule is enclosed by a cube (dimension $12.3\mu m \times 12.3\mu m \times 12.3\mu m$, see Figure 1b) used to mimic a portion of the ventricular myocyte, where the top face of the cube is treated as the cell surface membrane. The interior of the cube represents the cytosol. In this study, the Ca^{2+} dynamics in ventricular myocytes is investigated by considering three separate geometric cases (see Figure 1b): (a) the realistic T-tubule is placed close to the surface membrane represented by the top face of the surrounding cube; (b) the realistic T-tubule is placed at a distance of about $3\mu m$ away from the surface membrane; and (c) the realistic T-tubule is placed at a distance of about $6\mu m$ away from the

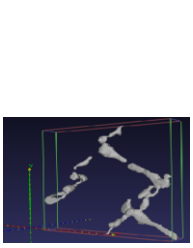

(a)

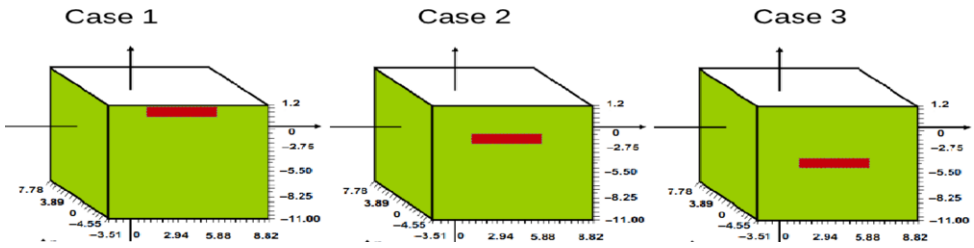

(b)

Fig. 1. (a) A realistic T-tubule obtained from 3D electron microscopy images (courtesy of Masahiko Hoshijima, UCSD). (b) Three different geometric models are developed by considering three different ways of locating the T-tubule. They are denoted as Case 1, Case 2, and Case 3. Here for ease of representation, T-tubule is represented by a red rectangle and for the three cases, the T-tubule is placed along the central axis and its distance from the cell surface (the top face in white) is as shown here. The red rectangle was not used in the numerical simulations but is used here to illustrate the positioning of the T-tubule in Fig. 1a.

surface membrane. These three different model geometries were used in numerical experiments to study the effect of geometric models on predicted Ca^{2+} dynamics.

2.1. The mathematical model

We consider the diffusion and association of Ca^{2+} with the endogenous stationary Ca^{2+} buffer (troponin C) and mobile buffers (ATP and Calmodulin) and with the exogenous mobile buffer (Fluo). For the sake of simplicity, it is assumed that Ca^{2+} binds to the buffers without cooperativity [8].

$$\frac{\partial [Ca^{2+}]_i}{\partial t} = D_{Ca}\nabla^2[Ca^{2+}]_i - \sum_{m=1}^{3} R_{B_m} - R_{B_s} + J_{Ca_{\text{flux}}} \qquad \text{in } \Omega \subset \mathbb{R}^3 \times (0,T), \tag{1}$$

$$\frac{\partial [CaB_m]}{\partial t} = D_{CaB_m}\nabla^2[CaB_m] + R_{B_m} \qquad \text{in } \Omega \subset \mathbb{R}^3 \times (0,T),\ m = 1,2,3, \tag{2}$$

$$\frac{\partial [CaB_s]}{\partial t} = R_{B_s} \qquad \text{in } \Omega \subset \mathbb{R}^3 \times (0,T), \tag{3}$$

where the reaction kinetics R_{B_s} and R_{B_m} $(m = 1,2,3)$ are defined as follows:

$$R_{B_s} = k_+^s([B_s] - [CaB_s])[Ca^{2+}]_i - k_-^s[CaB_s], \tag{4}$$

$$R_{B_m} = k_+^m([B_m] - [CaB_m])[Ca^{2+}]_i - k_-^m[CaB_m], \tag{5}$$

with $[B_m], m = 1,2,3$ and $[B_s]$ representing the total concentration of Fluo-3, calmodulin, ATP and troponin C respectively. The rate coefficients k_+^s and k_+^m $(m = 1,2,3)$ are the Ca^{2+} on-rate constants for troponin C, Fluo-3, calmodulin and ATP respectively and the rate coefficients k_-^s and k_-^m $(m = 1,2,3)$ are the Ca^{2+} off-rate constants for troponin C, Fluo-3, calmodulin and ATP respectively. Values of Ca^{2+} and buffer reaction-diffusion parameters are consistent with those given in Lu *et al* [8].

In (1), $J_{Ca_{\text{flux}}}(\mu M/ms)$ describes the total Ca^{2+} flux through the cell surface and the T-tubule. A reflective boundary condition is specified for (1) - (3).Experimental observations have shown that the stationary buffer troponin C does not reside on the cell membrane. Thus in this study troponin C is distributed only in the cytosol. We assume that the mobile buffers diffuse and react throughout the cytoplasm and cell membrane [8]. The resting Ca^{2+} concentration is taken to be $0.1\mu M$ [14]. The kinetics satisfies the equilibrium condition $R_{B_m} = R_{B_s} = 0$ and gives the following initial conditions, $[CaB_1] =$

$11.917\mu M$, $[CaB_2] = 0.968\mu M$, $[CaB_3] = 0.130\mu M$, $[CaB_s] = 6.364\mu M$. Following [10], we define the $J_{Ca_{\text{flux}}}$ through the cell surface and T-tubule as: $J_{Ca_{\text{flux}}} = J_{Ca} + J_{NCX} - J_{pCa} + J_{Cab}$, where J_{Ca} denotes the total Ca^{2+} influx via the L-type Ca^{2+} channels (LCCs), J_{NCX} the total Ca^{2+} influx (or efflux) via the Na^{+}- Ca^{2+} exchangers (NCXs), J_{pCa} the total Ca^{2+} pumps efflux and J_{Cab} the total background Ca^{2+} leak influx. In order to compute the value of the fluxes J_{Ca}, J_{NCX}, J_{pCa} and J_{Cab} we define their respective current densities I_{Ca}, I_{NCX}, I_{pCa} and I_{Cab}. I_{NCX} and I_{Cab} are functions of the holding potential of voltage-clamp protocol V: with $V = 10\,mV$, for $t \in (0,\ 70\,ms]$, and $V = -50\,mV$, for $t \in (70\ ms,\ \infty]$, (see Yao *et al* [10]) The given current densities I_i $(\mu M/ms)$, $i = Ca,\ NCX,\ pCa,\ Cab$ are converted to Ca^{2+} influx/efflux $J_i(\mu M/ms),\ i = Ca,\ NCX,\ pCa,\ Cab$ by using an experimentally estimated capacitance to rendered volume ratio, $(C_m/V_{cell} = 8.8\,pF/pL)$ in adult rat ventricular myocytes [10]:

$$J_i = \beta_i \frac{V_{mc}}{S_j} \left(\frac{1}{2F} \frac{C_m}{V_{cell}} \right) I_i, \tag{6}$$

where C_m (pF) is the cell capacitance, V_{cell} (pL) is the cell volume, V_{mc} (μm^3) is the compartment volume of the geometric model used to represent the cell in the numerical experiment, S_j (μm^2) is the total surface area where the channel i resides in the geometric model, F is the Faraday's constant, and $\beta_i,\ i = Ca,\ NCX,\ pCa,\ Cab$ is a model-dependent scaling parameter for LCCs, NCXs, Ca^{2+} pumps and background leak respectively. The values of the scaling parameters are as follows $\beta_{Ca} = 232.3$, $\beta_{NCX} = 133.7$, $\beta_{pCa} = 390.0$, and $\beta_{Cab} = 1345.0$. Immunohistochemical studies have shown marked variations in the distribution of Ca^{2+}- transporting protein complexes along the T-tubule and the sarcolemma [11,15,16]. In order to account for these variations we let I_{NCX} on the T-tubule to be three times of that on the surface membrane and I_{pCa} is zero on the cell surface.

2.2. Numerical computations

Numerical computations of the model is done using first-order backward Euler finite difference scheme (1-SBEM) [17] and finite element method (FEM) [18] for the time discretization and the spatial discretization respectively. The number of elements of the finite element mesh was chosen to be very large (i.e > $362,035$ elements) and a time-step of $0.01\ ms$ was used in order to obtain convergence. That is there was no significant difference among numerical solutions computed with time-step greater that $0.01\ ms$. In all three cases, an adaptive mesh is used with greater resolution on and near the T-tubule. The implementation of the numerical scheme was carried out in ALBERTA [21], a finite element toolbox. The simulation results were visualized using ParaView [22] visualization toolbox. Post-processing and data analysis were carried out in MATLAB version 7.7.0 (R2008b) [23].

3. Simulation results

The voltage-clamp protocol and the whole cell L-type Ca^{2+} current (LCC) used in the simulations are shown in Figure 2(a) and (b) respectively. In Figure 2(c)-(i), blue, green and red represent the results obtained for case 1, case 2 and case 3 respectively. Ca^{2+} extrusion occurs only via Ca^{2+} pumps between $(0,\ 70\ ms]$. After $70\ ms$ there is a combined extrusion of Ca^{2+} by both Na^{+}/Ca^{2+} exchangers and Ca^{2+} pumps, while Ca^{2+} influx occurs via the Ca^{2+} background leaks. In this model the predicted Na^{+}/Ca^{2+} current efflux obtained after the blockade of LCCs is slightly different for each of the three

cases considered here (see Figure 2(c), a negative NCX value signifies an efflux of Ca^{2+} ions via NCX while a positive value signifies an influx of Ca^{2+} ions via NCX). The profile of the global Ca^{2+} transient is also different for the three cases (see Figure 2(f)), for case 1, the global Ca^{2+} transients peaked at approximately 70 ms and then begins to decrease after the blockade of LCC. In case 2, the concentration of the global Ca^{2+} is lower compared to that in case 1 (see Figure 2(f)).It peaks and then stays fairly constant at approximately 184 ms. That is, the global Ca^{2+} transient continues to increase for a while after the complete blockade of the LCC currents. In case 3, the predicted global Ca^{2+} transient is significantly different from those obtained in the other cases (see Figure 2(f)) and is increasing throughout the simulation time. The trend in this model is that as the distance between the T-tubule and the cell surface increases, the global Ca^{2+} peak time increases.

The Ca^{2+} pump and NCX current for all three cases (see Figure 2(c), (d)) have transient profiles (i.e curves) that show a direct proportional relationship with their respective global Ca^{2+} transient profiles. Note that when Ca^{2+} pump and NCX current are fairly constant, then global Ca^{2+} will stay equally constant. Also when Ca^{2+} pump and NCX current are increasing (or decreasing) then global Ca^{2+} will be increasing (or decreasing). The model did not produce any significant difference among the predicted Ca^{2+} leak for the three cases (see Figure 2(e)). Figure 2(g)-(i) are the predicted concentrations of CaFluo, CaCal and CaATP, which increases with increasing free Ca^{2+} and peak at approximately the same time as the Ca^{2+} transient peak (see Figure 2(f)-(i)). This is consistent with experiment observations that the buffer dynamics is dependent on the available Ca^{2+} concentration.

Furthermore, a scanned line AB, is located in close proximity to the T-tubule and begins from the top surface of the box (which represents the cell surface) and ends at about 6.52 μm away from the top surface. Using this scanned line, the local Ca^{2+} concentrations in the model cell is studied. The scanned line image for the local Ca^{2+} concentration is shown in Figure 2(j)-(l) for cases 1, 2 and 3 respectively. In all three cases, a high Ca^{2+} gradient is observed close to the cell surface but a higher peak value is observed close to the cell surface in cases 2 and 3.

3.1. Comparing the predicted local Ca^{2+} concentrations in the three geometric models

Figure 3(a)-(c) are cross-sectional views of Ca^{2+} concentration distribution at 70 ms for the three different cases. In case 1, the Ca^{2+} concentration is lower on the cell surface in comparison to the other two cases. In order to study further the Ca^{2+} variations, diagonal lines is placed on the cell surface of the geometric model for each case and plot the Ca^{2+} concentration along these lines (see Figure 3d). Furthermore, in each of the three geometric models, Ca^{2+} concentration at a feature point located at the center of the cell surface is plotted against time (see Figure 4a). Observe that the Ca^{2+} concentration for case 1 differs greatly from those of the other two case. Recall that in case 1, the T-tubule is placed very close to the cell surface and around the centre, which is where a lower Ca^{2+} concentration is observed (see Figure 3(a)). Based on these results, one can infer that when the T-tubule is located close to the cell surface then we have a lower accumulation of Ca^{2+} on the surface and the average Ca^{2+} concentration in the cell model is higher when compared to the other two cases. This implies that when the T-tubule and cell surface contribute Ca^{2+} together at close proximity then the average Ca^{2+} concentration will be maximized.

3.2. Predicted free Ca^{2+} concentrations in the absence of buffers

In the absence of buffers activity, the highest free Ca^{2+} concentrations is obtained in the model that has T-tubule located close to the cell surface (see Figure 4b, blue graph). Also after the blockage of LCCs,

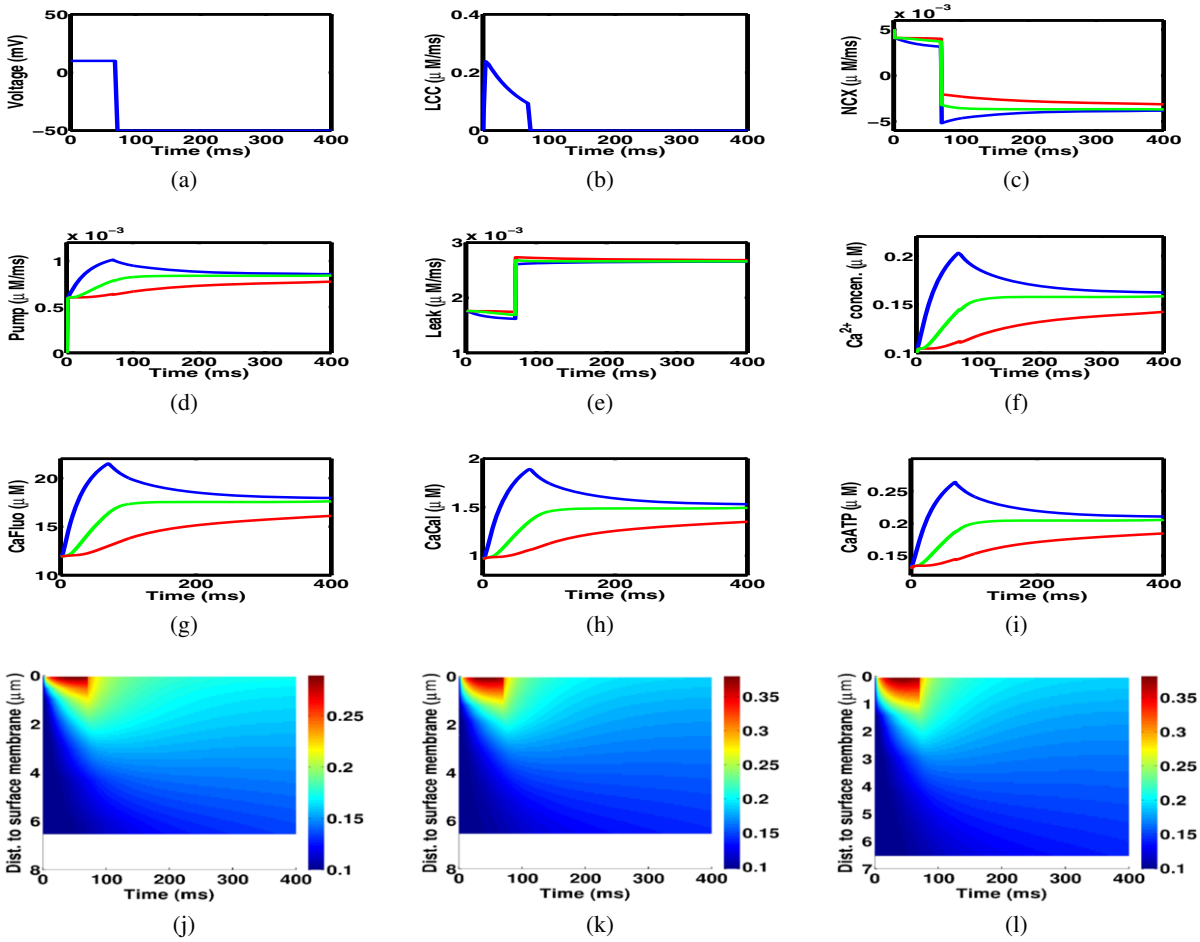

Fig. 2. Simulation results for the model. (a) and (b) The voltage-clamp protocol and the whole-cell L-type Ca^{2+} current (LCC) used in the simulations. In (c)-(i), blue, green and red represent the results obtained for case 1, case 2 and case 3 respectively. (c)-(f) The predicted global Na^{+}/Ca^{2+}, Ca^{2+} pump, Ca^{2+} leak currents and global Ca^{2+} transients respectively. (g)-(i) The predicted concentrations of CaFluo, CaCal and CaATP respectively. (j)-(l) Line-scan images of Ca^{2+} concentrations visualized in transverse cell direction and located perpendicular to the cell surface for cases 1, 2 and 3 respectively.

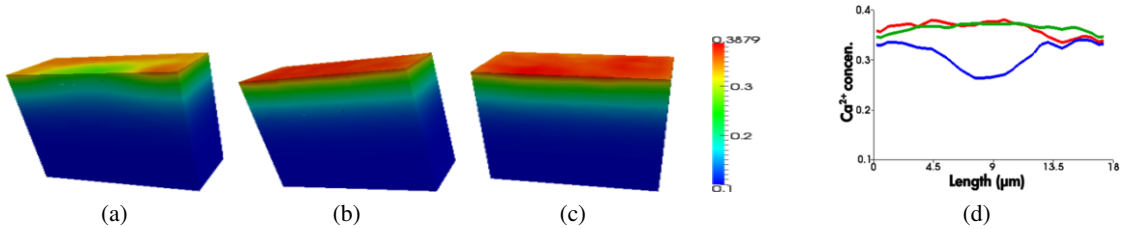

Fig. 3. 3D view of Ca^{2+} concentration distribution at 70 ms for the three different cases. (a) Case 1, the model with T-tubule near the cell surface, (b) Case 2, the model with T-tubule in the middle from the top to the center of the box, (c) Case 3, the model with T-tubule in the center of the box.(d) Ca^{2+} concentration at 70 ms plotted along a diagonal line on the cell surface. Blue, green and red represent the results obtained for case 1, case 2 and case 3 respectively.

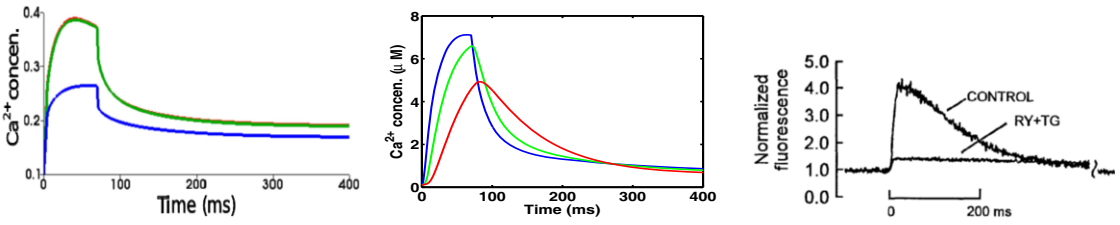

(a)

Fig. 4. Ca^{2+} transient. (a) A feature point at the centre of the cell surface is chosen and the Ca^{2+} concentration at this point is plotted over time. (b) Predicted free Ca^{2+} transients from the blockade of all buffers. Blue, green, red corresponds cases 1, 2, 3 respectively. (c) Depolarization-activated Ca^{2+} transients [19], reproduced with permission from Springer-Verlag.

the efflux of Ca^{2+} from the cytosol is slower for the model with T-tubule in the center of the cell model. This is partly because in the models, pumps were located only on the cell surface but not on the T-tubule. Another reason is that the Ca^{2+} efflux is maximized only when the T-tubule is placed close to the surface membrane. In this case the combined efflux via the cell surface and T-tubule efflux channels is highly efficient due to their close proximity. Figure 4b also shows that the available free Ca^{2+} concentration is very high after the blockade of buffers, thus highlighting the importance of buffers in the regulation of Ca^{2+} concentration in the cytosol.

3.3. Comparison with experimental observations

In Cheng *et al* [19], Ca^{2+} transients in isolated rat heart cells was studied by using a laser scanning conformal microscope and the Ca^{2+} indicator Fluo-3. In their study, the SR Ca^{2+} release channel was blocked with 1 μM ryanodine and SR Ca^{2+} uptake was inhibited with 1 μM thapsigargin. The Ca^{2+} transient was studied under control conditions and also after the exposure of the myocyte to 1 μM ryanodine and 1 μM thapsigargin (RY+TG). The rat ventricular myocyte was loaded with 100 μM Fluo-3 and subjected to electrical simulation to mimic *in-vivo* conditions. Ca^{2+} transient was then recorded along a single confocal scan line. Under control conditions, the normalized peak fluorescence was about 4.1 μM corresponding to a Ca^{2+} concentration of about 1.82 μM. After exposure to ryanodine and thapsigargin the peak of the normalized fluorescence was reduced to 1.45 μM corresponding to a peak Ca^{2+} concentration of about 0.163 μM [19] (see Figure 4c, reproduced with permission from Springer-Verlag). Recall that in case 1, the T-tubule was located to somehow imitate the experimental observations of T-tubule as invaginations of the cell membrane. Comparison of the Ca^{2+} transient for Case 1 (see Figure 2 (f), blue curve) with the experiment by Cheng *et al* [19] shows that the decay of Ca^{2+} was faster for case 1. A reason for this could be due to the fact that in the simulations, a constant extracellular Na^{+} concentration of 140 mM was assumed. The choice of extracellular Na^{+} is known to affect the predicted decay of Ca^{2+} in numerical simulations [9]. In the study by Cheng *et al* [9], numerical simulations were carried out using different concentrations of extracellular Na^{+} and they observed that a reduction in the value of the extracellular Na^{+} concentration can reduce the rate of decay of Ca^{2+} in the simulation.

4. Conclusion

The intracellular Ca^{2+} concentration plays a key role during excitation-contraction coupling in cardiac myocytes. In this work, three geometric models with realistic T-tubule were used to study the effect of

T-tubule location on Ca^{2+} transient. In one geometric model the T-tubule was located very close to the cell surface and in the other two geometric models the T-tubule was located at approximately 3 μm and 6 μm away from the cell surface. This result suggests that the location of T-tubule is vital in the regulation of Ca^{2+} concentrations in the cell. Also the difference in the predicted Ca^{2+} concentrations in the three geometric models highlight that the choice of geometric model is critical in the simulation of Ca^{2+} dynamics in ventricular myocytes. In summary, one can infer that the location and structure of the T-tubule play a key role in Ca^{2+} regulation in ventricular myocytes.

References

[1] K. Acsai, G. Antoons, L. Livshitz, Y. Rudy, and K. R. Sipido. Microdomain [Ca^{2+}] near ryanodine receptors as reported by L-type Ca^{2+} and Na^{+}/Ca^{2+} exchange currents. *J. Physiol.*, 589(Pt 10):2569–2583, 2011.

[2] Donald M. Bers. Calcium fluxes involved in control of cardiac myocyte contraction. *Circulation Research*, 87(4):275–281, 2000.

[3] C. Allyson Walker and Francis G. Spinale. The structure and function of the cardiac myocyte: A review of fundamental concepts. *J Thorac Cardiovasc Surg*, 118(2):375–382, 1999.

[4] Arnold M. Katz. *Physiology of the heart*. Raven Press, New York, 1977.

[5] J. N. Weiss. Ion channels in cardiac muscle. In G. A. Langer, editor, *The Myocardium*. Academic Press, San Diego, second edition, 1997.

[6] Beat Schwaller. Cytosolic Ca^{2+} buffers. *Cold Spring Harb. Perspect. Biol.*, 2(11), 2010. DOI: 10.1101/cshperspect.a004051.

[7] Alex Sirker and Ajay M. Shah. Biochemistry and physiology of cardiac muscle. *Medicine*, 38(7):340 – 343, 2010.

[8] L. Shaoying, A. Michailova, J. Saucerman, Y. Cheng, Z. Yu, T. Kaiser, W. Li, R. Bank, M. Holst, J. Mccammon, T. Hayashi, M. Hoshijima, P. Arzberger, and A. McCulloch. Multiscale modeling in rodent ventricular myocytes. *Engineering in Medicine and Biology Magazine, IEEE*, 28(2):46 –57, march-april 2009.

[9] Y. Cheng, Z. Yu, M. Hoshijima, M. J. Holst, A. D. McCulloch, J. A. McCammon, and A. P. Michailova. Numerical analysis of Ca^{2+} signaling in rat ventricular myocytes with realistic transverse-axial tubular geometry and inhibited sarcoplasmic reticulum. *PLoS Comput Biol*, 6(10):e1000972, 2010.

[10] Guangming Yao and Zeyun Yu. A localized meshless approach for modeling spatial-temporal calcium dynamics in ventricular myocytes. *International Journal for Numerical Methods in Biomedical Engineering*, 28(2):187–204, 2012.

[11] F. Brette and C. Orchard. T-tubule function in mammalian cardiac myocytes. *Circulation Research*, 92:1182–1192, 2003.

[12] Savio-Galimberti E., Frank J., Inoue M., Goldhaber J. I., Cannell M. B., Bridge J. H., and Sachse F. B. Novel features of the rabbit transverse tubular system revealed by quantitative analysis of three-dimensional reconstructions from confocal images. *Biophys. J.*, 95:2053–2062, 2008.

[13] M. Ibrahim, J. Gorelik, M. H. Yacoub, and C. M. Terracciano. The structure and function of cardiac t-tubules in health and disease. *Proceedings of the Royal Society B: Biological Sciences*, 278:2714–2723, 2011.

[14] Donald Bers. *Excitation-Contraction Coupling and Cardiac Contractile Force*. Developments in Cardiovascular Medicine. Springer, 1993.

[15] M. Pásek, F. Brette, A. Nelson, C. Pearce, A. Qaiser, G. Christe, and C.H. Orchard. Quantification of t-tubule area and protein distribution in rat cardiac ventricular myocytes. *Progress in Biophysics and Molecular Biology*, 96(1-3):244 – 257, 2008.

[16] David R.L. Scriven, Pauline Dan, and Edwin D.W. Moore. Distribution of proteins implicated in excitation-contraction coupling in rat ventricular myocytes. *Biophysical Journal*, 79(5):2682 – 2691, 2000.

[17] A. Madzvamuse. Time-stepping schemes for moving grid finite elements applied to reaction-diffusion systems on fixed and growing domains. *J. Comput. Phys.*, 214(1):239–263, 2006.

[18] J. N. Reddy. *An introduction to the finite element method*. McGraw-Hill, New York, 1993.

[19] H. Cheng, M. B. Cannell, and W. J. Lederer. Propagation of excitation-contraction coupling into ventricular myocytes. *Pflugers Arch*, 428:415–417, 1994.

[20] S. Wei, A. Guo, B. Chen, W. J. Kutschke, Y-P. Xie, K. Zimmerman, R. M. Weiss, M. E. Anderson, H. Cheng, and L-S. Song. T-tubule remodeling during transition from hypertrophy to heart failure. *Circ. Res.*, 107(4):520–531, 2010.

[21] A. Schmidt, K. G. Siebert, D. Köster, and C. Heine. *Design of adptive finite element software: The finite element toolbox ALBERTA*, 11 December 2006. Version: ALBERTA-2.0.

[22] A. Henderson. *ParaView Guide: A Parallel Visualization Application*. Kitware Inc., 2004.

[23] MATLAB. *version 7.7.0 (R2008b)*. The MathWorks Inc., Natick, Massachusetts, 2008.